Journal of Engineering Physics and Thermophysics, Vol. 83, No. 2, 2010

TURBULENT REGIME OF THERMOGRAVITATIONAL CONVECTION IN A CLOSED CAVITY

G. V. Kuznetsov[a] **and M. A. Sheremet**[b]

UDC 669.86:536.21

We have performed a numerical analysis of the nonstationary turbulent natural convection in a closed region with heat-conducting walls of finite thickness and a heat source located at the cavity base under the conditions of convective-radiative heat exchange with the environment. Typical distributions of the thermohydrodynamic parameters (streamlines, temperature field, field of the kinetic energy of turbulence, and dissipation field of the kinetic energy of turbulence) in a fairly wide range of Grashof numbers $10^7 \le Gr \le 10^9$ have been obtained. Results characterizing the scales of influence of the nonstationarity factor and the relative heat conductivity coefficient of the material of the surrounding walls on the heat transfer intensity are presented. A correlation for determining the average Nusselt number on the heat source surface has been established.

Keywords: *conjugate heat transfer, turbulence, natural convection, heat source, closed region.*

Introduction. Modern objects of radioelectronic equipment and electronic engineering (REE and EE) must satisfy stringent requirements, where an important role is played by precision, reliability, and stability of operation [1–7]. The range of problems solved by electronic devices presupposes employment of typical REE and EE units and assemblies in a wide range of thermal actions. Among the main factors destabilizing the optimal operating conditions of REE and EE devices and leading to a deviation of input characteristics from nominal values are various kinds of thermal action: ambient temperature, external thermal flows, power of internal energy sources. A characteristic feature of REE and EE devices is the conversion of a significant portion (up to 10%) of input energy into thermal energy. Released energy increases the temperature of elements and lowers their reliability, distorts the useful signal, or even makes the device inoperative.

An increase in the temperature from 20 to 80^{o}C leads to an increase in the intensity of failures of semiconductor devices by a factor of 3–4, resistors by a factor of 2–3, capacitors by a factor of 6–8, and integrated circuits by a factor of 6–10 [5–7].

In developing modern microelectronic devices characterized by high local specific thermal loads, it is necessary to take into account the main thermophysical processes proceeding in the gas cavity of a typical REE and EE assembly or unit. Therefore, design of radioelectronic and electronic equipment presupposes thorough treatment of a structure providing a rational arrangement of units, the necessary heat transfer intensity, and the possibility of thermostabilization of the most temperature-sensitive parts and elements.

The aim of the present work is mathematical modeling of turbulent thermal conditions in a typical REE or EE component under inhomogeneous heat exchange with the environment.

Mathematical Model. A boundary-value conjugate problem of nonstationary turbulent heat transfer in a closed square region (Fig. 1) is considered. The investigated region is typical of the majority of REE and EE elements in the presence of an internal heat source located at the base of the gas cavity.

The solution region represents a gas cavity bounded from the environment by heat-conducting finite-thickness walls. The heat source located in the bottom part of the cavity has a constant temperature. The outer surfaces of the enclosing walls ($y = 0$, $y = L_y$, $x = L_x$) are supposed to be heat-insulated. At the boundary $x = 0$ simultaneous radiative-convective heat exchange with the environment is realized.

It is assumed that the thermophysical properties of the wall material and the gas are temperature independent and the flow conditions are turbulent. The gas is assumed to be a viscous, heat-conducting Newtonian fluid satisfying

[a]Tomsk Polytechnical University, 30 Lenin Ave., Tomsk, 634050, Russia; [b]Tomsk State University, 36 Lenin Ave., Tomsk, 634050, Russia; email: Michael-sher@yandex.ru. Translated from Inzhenerno-Fizicheskii Zhurnal, Vol. 83, No. 2, pp. 326–337, March–April, 2010. Original article submitted February 23, 2009.

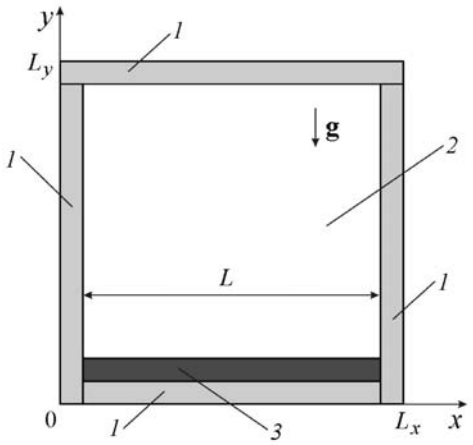

Fig. 1. Solution region of the problem: 1) walls; 2) gas; 3) heat source.

the Boussinesq approximation. The gas flow and the heat transfer in the internal volume are assumed to be two-dimensional, the heat exchange of radiation from the heat source and between the walls is assumed to be negligibly small compared to the convective heat exchange, and the gas is assumed to be transparent to thermal radiation. It is also assumed that the size on the third coordinate is much larger than on the other two coordinates and the end effects of the flow and the heat exchange are negligibly small; therefore, a two-dimensional formulation of the problem is considered.

The process of heat transfer in the considered region (Fig. 1) is described by a system of nonstationary two-dimensional equations of turbulent natural convection in the gas cavity [8–12] and by a nonstationary two-dimensional heat conduction equation for elements of the solid material [13] with nonlinear boundary conditions. As a closing turbulence model, we considered the well-studied k–ε model [10].

The boundary-value problem is formulated in the dimensionless variables stream function–velocity vorticity vector–temperature. For the scale distance, we chose the gas cavity length on the x-axis. To reduce the system of equations to dimensionless form, we used the following relations:

$$X = x/L\,,\quad Y = y/L\,,\quad \tau = t/t_0\,,\quad U = u/V_0\,,\quad V = v/V_0\,,\quad \Theta = (T - T_0)/\Delta T\,,$$

$$\Psi = \psi/\psi_0\,,\quad \Omega = \omega/\omega_0\,,\quad K = k/k_0\,,\quad E = \varepsilon/\varepsilon_0$$

at $\Delta T = T_{\mathrm{h.s}} - T_0$, $\psi_0 = V_0 L$, $\omega_0 = V_0/L$, $k_0 = V_0^2$, $\varepsilon_0 = V_0^3/L$.

The Reynolds equations in the dimensionless variables stream function–velocity vorticity vector together with the standard k–ε model of turbulence have the following form [14, 15]:

for the gas (2 in Fig. 1)

$$\frac{\partial^2\Psi}{\partial X^2} + \frac{\partial^2\Psi}{\partial Y^2} = -\Omega\,, \tag{1}$$

$$\frac{\partial\Omega}{\partial\tau} + U\frac{\partial\Omega}{\partial X} + V\frac{\partial\Omega}{\partial Y} = \frac{\partial^2}{\partial X^2}\left[\left(\frac{1}{\sqrt{\mathrm{Gr}}} + \frac{1}{\mathrm{Re_t}}\right)\Omega\right] + \frac{\partial^2}{\partial Y^2}\left[\left(\frac{1}{\sqrt{\mathrm{Gr}}} + \frac{1}{\mathrm{Re_t}}\right)\Omega\right] + \frac{\partial\Theta}{\partial X}$$

$$+ 2\frac{\partial U}{\partial Y}\frac{\partial^2}{\partial X^2}\left(\frac{1}{\mathrm{Re_t}}\right) - 2\frac{\partial V}{\partial X}\frac{\partial^2}{\partial Y^2}\left(\frac{1}{\mathrm{Re_t}}\right) + 2\left(\frac{\partial V}{\partial Y} - \frac{\partial U}{\partial X}\right)\frac{\partial^2}{\partial X\partial Y}\left(\frac{1}{\mathrm{Re_t}}\right), \tag{2}$$

$$\frac{\partial\Theta}{\partial\tau} + U\frac{\partial\Theta}{\partial X} + V\frac{\partial\Theta}{\partial Y} = \frac{\partial}{\partial X}\left[\left(\frac{1}{\mathrm{Pr}\sqrt{\mathrm{Gr}}} + \frac{1}{\mathrm{Pr_t\,Re_t}}\right)\frac{\partial\Theta}{\partial X}\right] + \frac{\partial}{\partial Y}\left[\left(\frac{1}{\mathrm{Pr}\sqrt{\mathrm{Gr}}} + \frac{1}{\mathrm{Pr_t\,Re_t}}\right)\frac{\partial\Theta}{\partial Y}\right], \tag{3}$$

TABLE 1. Values of the Average Nusselt Numbers

Ra	Obtained reuslts	Literature data		
		[19]	[20]	[21]
10^7	17.72	16.79	16.523	—
10^8	33.41	30.506	30.225	28.78
10^9	54.49	57.350	—	62.0

$$\frac{\partial K}{\partial \tau} + U\frac{\partial K}{\partial X} + V\frac{\partial K}{\partial Y} = \frac{\partial}{\partial X}\left[\left(\frac{1}{\sqrt{\mathrm{Gr}}} + \frac{1}{\sigma_k \mathrm{Re_t}}\right)\frac{\partial K}{\partial X}\right] + \frac{\partial}{\partial Y}\left[\left(\frac{1}{\sqrt{\mathrm{Gr}}} + \frac{1}{\sigma_k \mathrm{Re_t}}\right)\frac{\partial K}{\partial Y}\right] + P_k + G_k - E\,, \tag{4}$$

$$\frac{\partial E}{\partial \tau} + U\frac{\partial E}{\partial X} + V\frac{\partial E}{\partial Y} = \frac{\partial}{\partial X}\left[\left(\frac{1}{\sqrt{\mathrm{Gr}}} + \frac{1}{\sigma_\varepsilon \mathrm{Re_t}}\right)\frac{\partial E}{\partial X}\right] + \frac{\partial}{\partial Y}\left[\left(\frac{1}{\sqrt{\mathrm{Gr}}} + \frac{1}{\sigma_\varepsilon \mathrm{Re_t}}\right)\frac{\partial E}{\partial Y}\right] + c_{1\varepsilon}\,(P_k + c_{3\varepsilon}G_k)\,\frac{E}{K} - c_{2\varepsilon}\,\frac{E^2}{K}\,, \tag{5}$$

for the solid walls (1 in Fig. 1)

$$\frac{1}{\mathrm{Fo}_1}\frac{\partial \Theta_1}{\partial \tau} = \frac{\partial^2 \Theta_1}{\partial X^2} + \frac{\partial^2 \Theta_1}{\partial Y^2}\,. \tag{6}$$

The parameters of the standard k–ε model of turbulence [10] are:

$$c_\mu = 0.09\,,\quad c_{1\varepsilon} = 1.44\,,\quad c_{2\varepsilon} = 1.92\,,\quad c_{3\varepsilon} = 0.8\,,\quad \mathrm{Pr_t} = 1.0\,,\quad \sigma_k = 1.0\,,\quad \sigma_\varepsilon = 1.3\,.$$

For the formulated problem (1)–(6):

the initial condition

$$\Psi\,(X, Y, 0) = \Omega\,(X, Y, 0) = K\,(X, Y, 0) = E\,(X, Y, 0) = \Theta\,(X, Y, 0) = 0$$

holds on the heat source during the whole process $\Theta = 1$;

the boundary conditions at the boundary $x = 0$ take into account the heat exchange with the environment due to the convection and radiation

$$\frac{\partial \Theta_1}{\partial X} = \mathrm{Bi_1}\Theta_1 - \mathrm{Bi_1}\Theta_\mathrm{e} + \mathrm{Sk_1}\left[\left(\Theta_1 + \frac{T_0}{T_{\mathrm{h.s}} - T_0}\right)^4 - \left(\frac{T_\mathrm{e}}{T_{\mathrm{h.s}} - T_0}\right)^4\right],$$

on the other outer boundaries for the energy equation the heat insulation conditions

$$\frac{\partial \Theta_1\,(X, Y, \tau)}{\partial X^k} = 0\,,\quad X^1 \equiv X\,,\quad X^2 \equiv Y$$

are given; on the boundaries between the solid material and the gas parallel to the coordinate axes $0X(0Y)$ the following conditions are met:

$$\Psi = 0\,,\quad \frac{\partial \Psi}{\partial Y\,(\partial X)} = 0\,,\quad \Theta_1 = \Theta_2\,,\quad \frac{\partial \Theta_1}{\partial Y\,(\partial X)} = \lambda_{2,1}\frac{\partial \Theta_2}{\partial Y\,(\partial X)}\,,$$

and for the turbulent characteristics K and E on the solid boundaries the kinetics energy of turbulence is defined directly on the surface of the solid wall $K = 0$, and its dissipation rate is calculated in the nearest near-boundary unit $E = c_\mu^{3/4} / K^{3/2} / (0.42\ \mathrm{h})$ [16].

The boundary-value problem (1)–(6) was solved by the finite difference method [17, 18] on a uniform grid (150 × 150). For the numerical solution of Eqs. (2)–(6), the locally one-dimensional scheme of A. A. Samarskii [18] was used. To resolve the nonlinear boundary condition of kind III, we used the method of simple iterations. The Poisson equation (1) for the stream function was solved on the basis of the fast Fourier transform [17].

This solution method was tested on a model problem. We considered the turbulent natural convection in a closed region [19] with isothermal vertical and adiabatic horizontal walls. The average Nusselt number on the vertical wall served as the quantity to be determined (see the Table 1).

The results presented in the table vividly show that the employed numerical solution method leads to a fairly good agreement with the data of other authors.

Results and Discussion. We carried out numerical investigations of the boundary-value problem (1)–(6) with corresponding initial boundary conditions at the following values of the dimensionless complexes: $10^7 \le \mathrm{Gr} \le 10^9$, Pr = 0.7, $\lambda_{2,1}$ = 0.037, 0.0037. Primary consideration was given to the analysis of the influence of the Grashof number and the nonstationary factor, as well as of the relative heat conductivity coefficient $\lambda_{2,1}$, on the distributions of both the local characteristics (streamlines, temperature field, field of the kinetic energy of turbulence, and field of its dissipation rate) and the integral parameter (average Nusselt number on the heat source surface).

Influence of the Nusselt number. Figure 2 shows the streamlines, the temperature field, the field of the kinetic energy of turbulence, and the field of its dissipation rate at $\lambda_{2,1}$ = 0.037, τ = 600 corresponding to various values of the Grashof number. Arrows on the streamlines show the direction of gas flow.

Under turbulent conditions of conjugate heat transfer corresponding to $\mathrm{Gr} = 10^7$ (Fig. 2a), in the gas cavity two convective cells differing in both flow direction and scales of occupied regions are formed. The appearance of circulation flows is due to several reasons: the presence of a heat source, the intensity of conductive heat transfer in the walls, as well as the propagation of disturbances from the solid material elements. The first of these reasons shows up as the formation of a buoyancy force $\rho g_y \mathrm{Bu}$ as a result of the temperature drop in the zone of the cavity base. Over the heat source a thermal torch is formed. At an instant of time τ = 600 this torch approaches the surface of the first wall, which is due to the considerable cooling of the left element of the solid material. The lower-temperature front propagates far into the solution region from the boundary X = 0 due to the fact that the ambient temperature was lower than the initial temperature of the object being analyzed. On the inner surface of the left wall there is a significant growth of the temperature gradient intensifying the downflows of the gas, which in turn lead to a shift of the thermal torch. The heat source increases also the temperature of the solid material elements located near the heater surface. It should be noted that warming up of the left wall at $0.16 \le Y \le 0.26$ leads to an increase in the gas temperature in the region of the left corner of the cavity ($0.08 \le X \le 0.16$, $0.16 \le Y \le 0.26$). Such an effect of the conductive heat transfer in the solid material element on the convective heat transfer in the gas cavity shows up as a distinctive reflection of cold downflows of the gas. The deformation of the isotherm corresponding to the dimensionless temperature $\Theta = -0.1$ in the region of the base characterizes the heating of the left wall by the heat source.

The field of the kinetic energy of turbulence describes the turbulent flow intensity. The configuration of the lines K = const in the core with maximum kinetic energy values defines both the boundary between two convective cells and the direction of action of the thermal torch. In turn, the field of the dissipation rate of the kinetic energy of turbulence characterizes the zones of kinetic-to-thermal energy conversion. The dissipation rate acquires maximum values on the surfaces of the walls, and an increase in E in the region of the thermal torch is also noticeable.

A tenfold increase in the Grashof number (Fig. 2b) leads to marked changes in all thermohydrodynamic parameters. In the gas cavity, there is an increase in the sizes of the right convective cell, which inhibits to a certain extent the development of the left vortex. The thermal torch formed over the heat source is located at a distance from the surface of the right wall, which characterizes the increase in the torch stability against the action of the lower-temperature front from the boundary X = 0. The latter is also confirmed by the increase in the average temperature in the gas cavity. The configuration of isotherms reflects the gas flow in convective cells. The position of the thermal torch defines the boundary between two circulation flows. The core of the field of the kinetic energy of turbulence is concentrated thereby in the region of the right vortex, and the configurations of the lines K = const is analogous to the lines of flow of a larger-scale circulation. The dissipation field of the kinetic energy of turbulence changes slightly — the E value in the left part of the cavity decreases simultaneously with the formation of a distinctive core in the zone of the right convective cell. A slight redistribution of the intensive dissipation zones on the wall surfaces is observed.

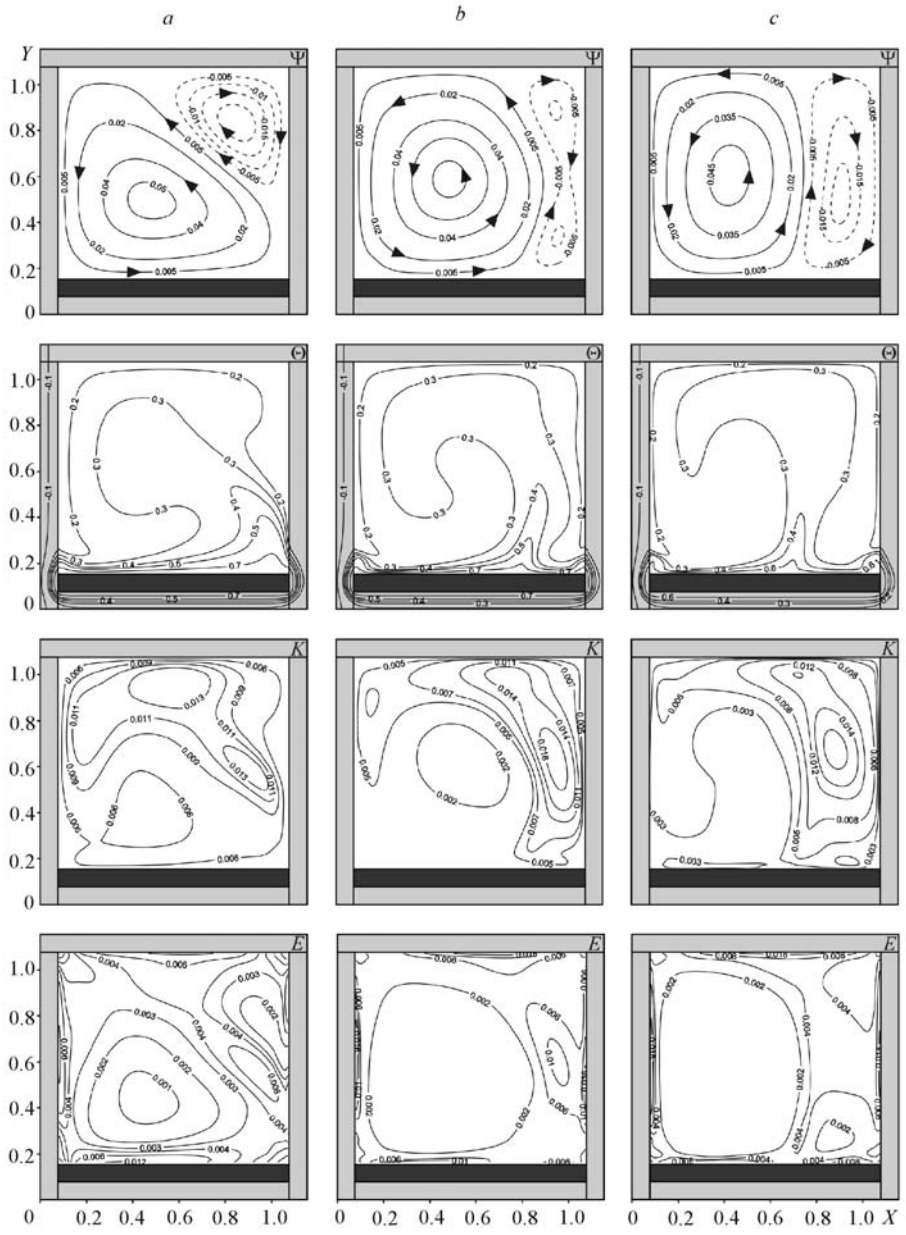

Fig. 2. Streamlines Ψ, temperature Θ field, field of the kinetic energy of turbulence K, and dissipation field of the kinetic energy of turbulence E at $\lambda_{2,1}$ = 0.037, τ = 600: a) Gr = 10^7; b) 10^8, c) 10^9.

A further increase in Gr (Fig. 2c) leads to a marked increase in the sizes of the vortex near the right element of the solid material. The thermal torch approaches the center of the gas cavity, reflecting the contact zone of two circulations. The conductive heat transfer intensification in the left and right walls in the zone of the heat source appears as the formation of secondary torches in the corner regions of the cavity. The field of the kinetic energy of turbulence undergoes structural changes — it increases in the scales of the turbulence initiation zone. The dissipation field of the kinetic energy of turbulence describes the increase in the sizes of the right vortex.

Thus, an increase in the Grashof number leads to an increase in the thermal torch stability, which tells on both the scales of the right convective cell and the position of the torch itself. The dissipation zones of the kinetic energy of turbulence incorporate not only the surfaces of the walls, but also, under certain conditions Gr = 10^7, 10^8, the region of the thermal torch.

Figure 3 shows the temperature profiles in different cross-sections of the solution region at Gr = 10^7, 10^8, and 10^9.

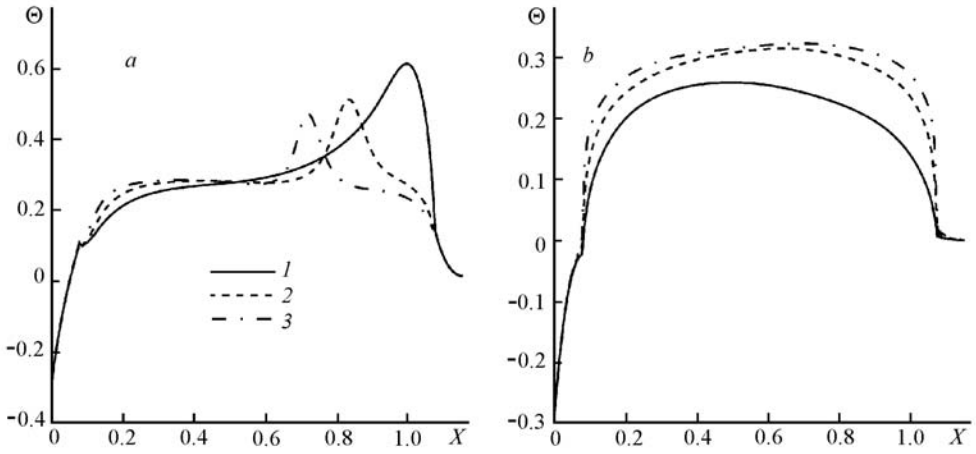

Fig. 3. Temperature profiles at $\lambda_{2,1} = 0.037$, $\tau = 600$ [$Y = 0.037$ — a), $Y = 1.0$ — b)]: 1) Gr = 10^7; 2) 10^8, 3) 10^9.

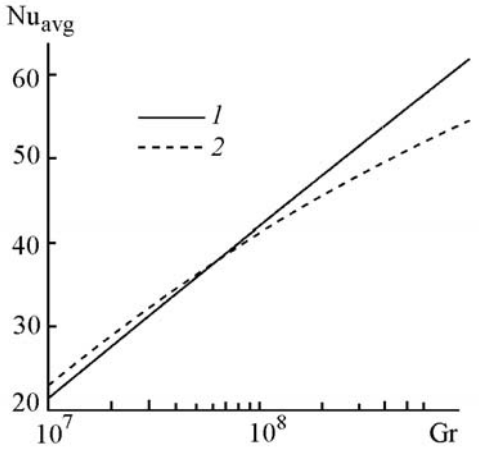

Fig. 4. Average Nusselt number versus the Grashof number at $\tau = 600$: 1) $\lambda_{2,1} = 0.037$; 2) 0.0037.

The temperature distributions complement the above analysis of the influence of the Grashof number. An increase in Gr leads to a shift of the thermal torch (maxima on the profiles) in the cross-section $Y = 0.31$ (Fig. 3a) to the symmetry plane of the cavity, and the temperature in the torches decreases therewith. The reason for the latter is the significant energy redistribution in the vertical direction. From Fig. 3b it is seen that in the upper parts of the gas cavity an increase in Gr shows up as a temperature increase.

The temperature increase in the zone $0.08 < X < 0.3$ (Fig. 3a) is due to not only to the shift of the thermal torch into the central region, but also the formation of a small thermal area in the left lower corner as a consequence of the influence of the conductive heat transfer on the convective heat transfer.

We have analyzed the influence of the Grashof number on the average Nusselt number on the heat source surface $\mathrm{Nu}_{\mathrm{avg}} = \int_{0.08}^{1.08} \left| \frac{\partial \Theta}{\partial Y} \right|_{Y=0.16} dX$.

Figure 4 shows graphically the increase in the generalized heat transfer coefficient with increasing Grashof number at a fixed value of the relative heat conductivity coefficient. This dependence can also be given in the form of the correlation relation $\mathrm{Nu}_{\mathrm{avg}} = 0.55\mathrm{Gr}^{0.23}$ at $\lambda_{2,1} = 0.037$. The increase in the average Nusselt number is due to the increase in the temperature gradient on the heat source surface, which is explained by the intensive energy removal by the cold downflows of the gas. This effect can also be traced by the distribution of isotherms in Fig. 2. An in-

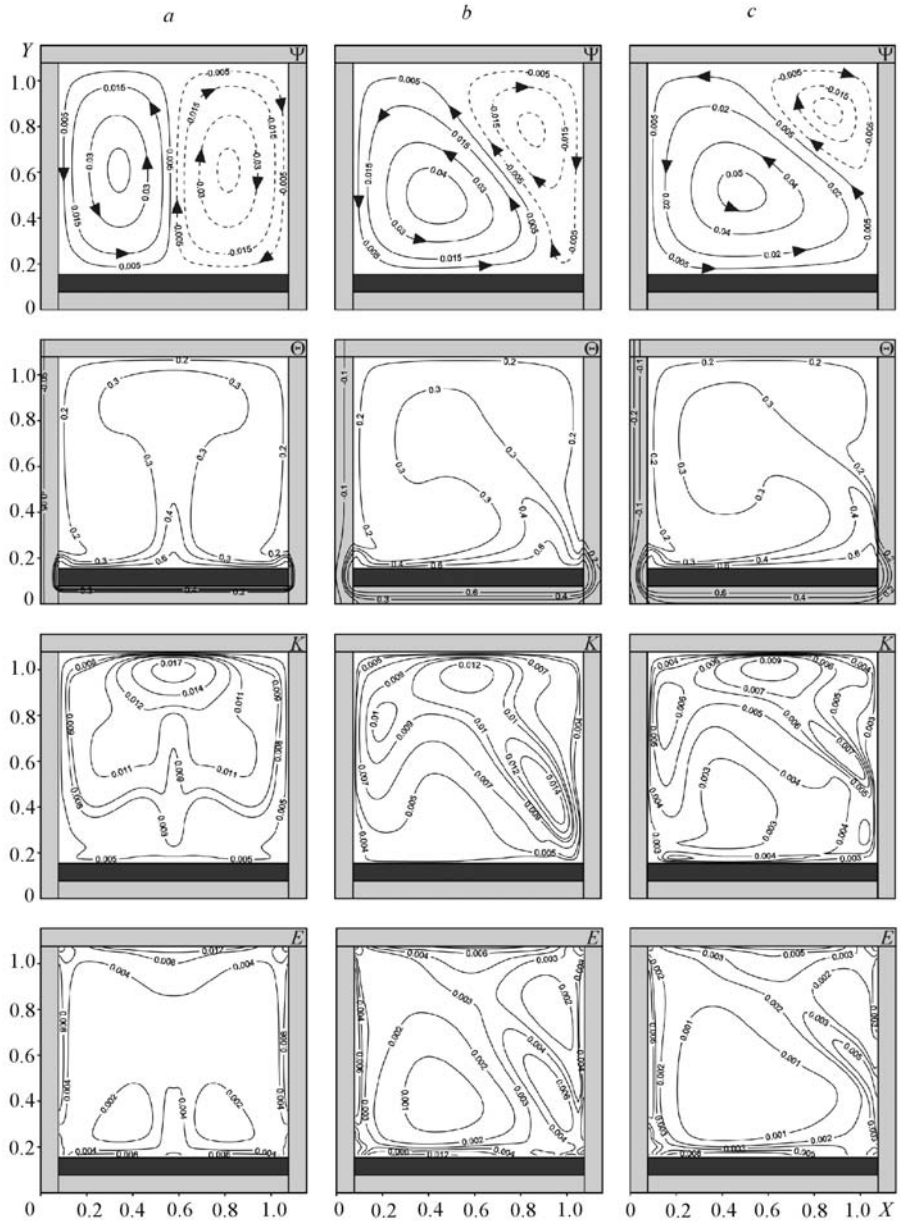

Fig. 5. Streamlines Ψ, temperature Θ field, field of the kinetic energy of turbulence K, and its dissipation field E at $\lambda_{2,1}$ = 0.037, Gr = 10^8: a) τ = 100; b) 700; c) 800.

crease in the Grashof number shows up as the approach of isotherms to the source surface and, accordingly, a decrease in the thickness of the thermal boundary layer.

Influence of the nonstationarity factor. The nonstationarity factor in the conjugate heat transfer problem plays an important role since it determines not only the moments of the formation, development, and dissipation of vortex structures in the gas cavity, but also the thermal inertia of the enclosing solid walls. The latter is most valuable in designing REE or EE components, as well as in optimizing the thermal regimes of electronic devices.

Figure 5 shows the streamlines, the temperature field, the field of the kinetic energy of turbulence, and its dissipation field at $\lambda_{2,1}$ = 0.37 and Gr = 10^8 at different instants of time.

At τ = 100 (Fig. 5a) in the gas cavity two convective cells differing in the direction of the gas flow are formed. The reason for the appearance of these vortices is the heat source forming over its surface a thermal torch extending along the vertical axis. The torch formed can be thought to be "starting" [22] since at the initial instant of

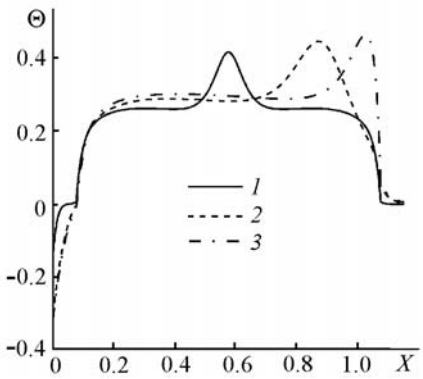

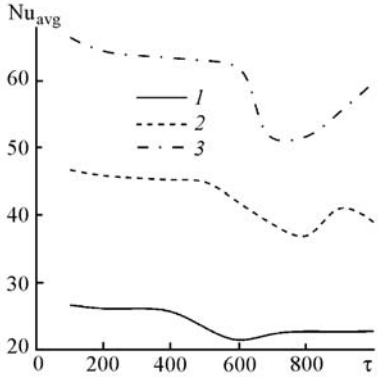

Fig. 6. Dimensionless temperature profiles at $Y = 0.4$, $\lambda_{2,1} = 0.037$, $Gr = 10^8$: 1) $\tau = 100$; 2) 700; 3) 800.

Fig. 7. Average Nusselt number versus the time and Grashof number at $\lambda_{2,1} = 0.037$: 1) $Gr = 10^7$; 2) 10^8, 3) 10^9.

time the gas is at rest and the energy source is switched on instantaneously. In the lower corner zones of the cavity, secondary starting torches are initiated due to the heating of the corresponding walls. A slight cooling of the left element of the solid material is also noticeable. The field of the kinetic energy of turbulence determines the "turbulization" zones. The K field core characterized by the maximum value of the energy of turbulence is located directly above the main starting torch. Zones of the highest dissipation rate of the energy of turbulence are, as before, the wall surfaces, and the propagation of disturbances from the upper wall far into the gas cavity is also noticeable, i.e., in the vicinity of the core of the kinetic energy of turbulence there is an increase in E. The symmetric distribution of all thermohydrodynamic parameters about the cross-section $X = 0.58$ is promoted by the initial time interval.

An increase in τ to 700 (Fig. 5b) leads to a more significant cooling of the left wall, which tells on the increase in the scales of the left convective cell which deforms the vortex near the right element of the solid material. The thermal torch shifts to the right wall as a consequence of the intensification of the cold downflows of the gas near the surface of the left element of the solid material. The core of both the field of the kinetic energy of turbulence and of its dissipation field characterizes the position of the starting torch.

A further increase in the time parameter (Fig. 5c) shows up both as an increase in the sizes of the left vortex and as a shift of the main starting torch to the right wall. Such hydrodynamic changes are due to the formation of a significant temperature gradient on the inner surface of the left wall as a consequence of the substantial advance of the lower-temperature front from the boundary $X = 0$. The configuration of the lines $K = \text{const} \geq 0.005$ is analogous to both the streamlines and the starting torch. Thus, with the help of the kinetic energy field we can follow the formation of vortex structures as well as the position of the thermal torch. The constant dissipation rate lines complement the above.

Figure 6 shows the temperature profiles in the cross-section $Y = 0.4$ at $Gr = 10^8$ at various instants of time. An increase in τ leads to an increase in the temperature in the gas cavity, and the thermal torch therewith shifts to the right wall with increasing temperature in it. At the boundary $X = 0$ cooling of the left element of the solid material occurs, which in the considered cross-section has a weak effect on the temperature distribution near the left wall. Figure 6 demonstrates graphically the warming-up of the right element of the solid material due to both the conductive heat transfer from the heat source and the convective heat transfer in the gas. The latter reason is the most weighty because of the position of the thermal torch.

Figure 7 shows the dynamics of the generalized heat transfer coefficient on the heat source surface at various values of the Grashof number. With increasing time the average Nusselt number decreases, which is due to the gradual heating of the closest gas layers and, accordingly, due to the decrease in the temperature gradient on the source surface.

At $\tau > 600$ nonmonotonicities in the Nu_{avg} distribution appear, which is due to the continuous restructuring of the temperature field.

Influence of the relative heat conductivity coefficient. As mentioned above, in developing modern equipment it is necessary to consider thoroughly the structure including not only the optimization of geometric parameters, but also the choice of the necessary structural material providing the required thermal operating conditions of the device.

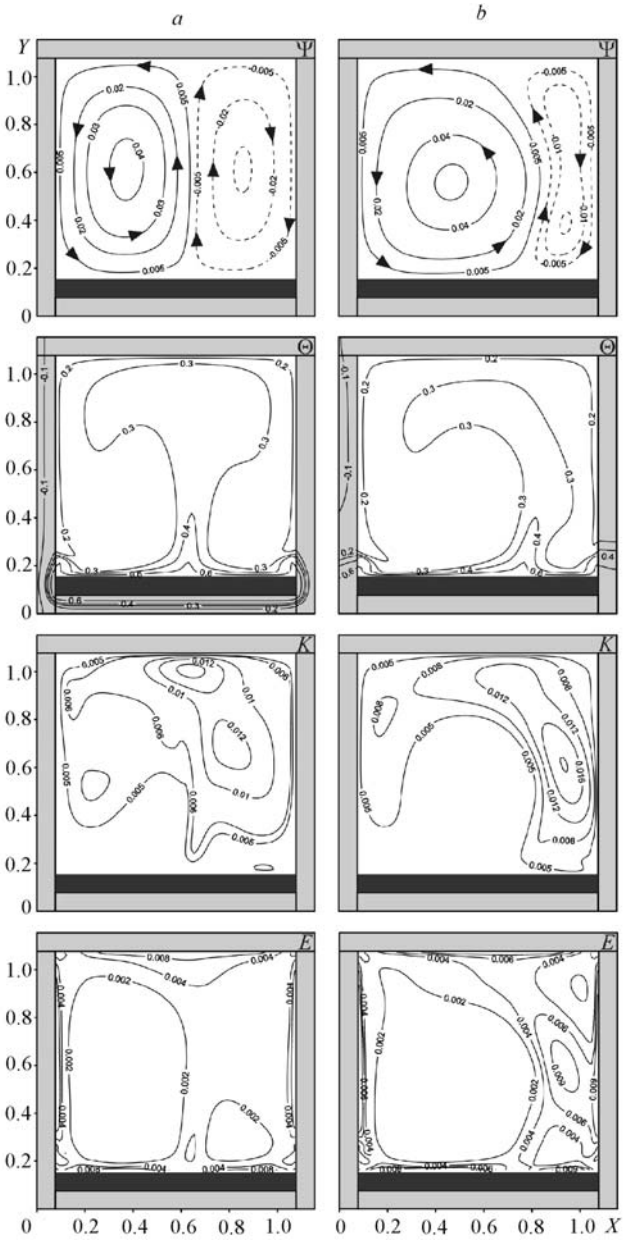

Fig. 8. Streamlines Ψ, temperature Θ field, field of the kinetic energy of turbulence K, and its dissipation field E at Gr = 10^9, τ = 500: a) $\lambda_{2,1}$ = 0.037; b) 0.0037.

Figure 8 presents the thermohydrodynamic parameters corresponding to the regime of convective heat transfer Gr = 10^9 at various values of the relative heat conductivity coefficients. The change-over from $\lambda_{2,1}$ = 0.037 to $\lambda_{2,1}$ = 0.0037 corresponds to a tenfold increase in the heat conductivity coefficient. Such a change leads to a redistribution of all diagnostic variables. The advance of the lower-temperature front becomes more substantial, which shows up as a shift of the thermal torch towards the right wall. There is an increase in both the scales of the left convective cell and the gas velocities in it. All this leads to a deformation of the vortex near the right wall. Cooling of the left element of the solid material occurs only in the zone $Y > 0.4$, which is due to the heating of the lower part by the heat source. The field of the kinetic energy of turbulence is somewhat modified — the core is shifted to the right wall and the configuration of the lines K = const reflects the orientation of the starting torch. The position and sizes of the convective cell can be related to the analogous parameters of the line of constant dissipation rate of the kinetic energy of turbulence corresponding to E = 0.02.

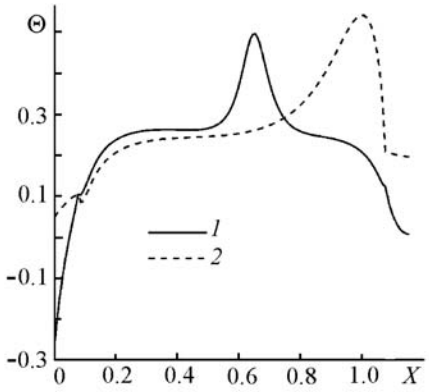

Fig. 9. Temperature profiles in the cross-section $Y = 0.3$ at $Gr = 10^8$, $\tau = 500$: 1) $\lambda_{2,1} = 0.037$; 2) 0.0037.

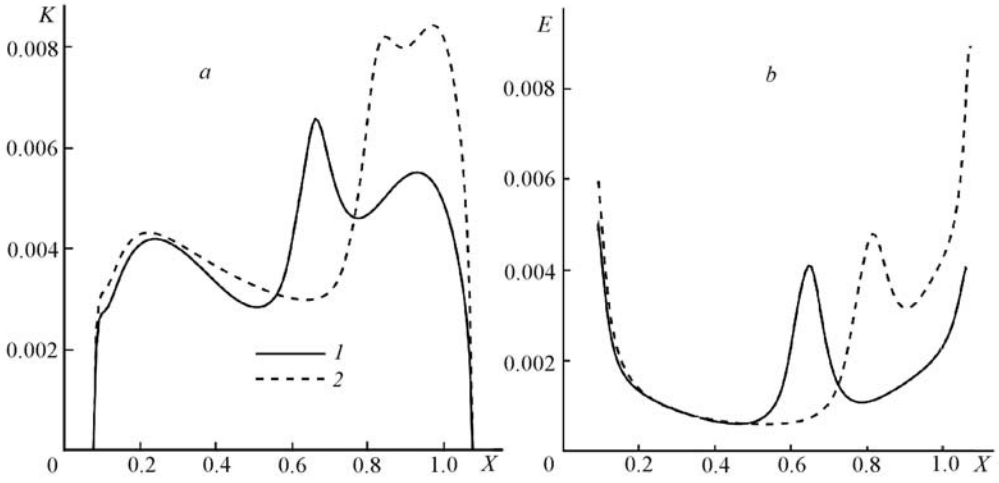

Fig. 10. Profiles of the kinetic energy of turbulence (a) and of its dissipation rate (b) in he cross-section $Y = 0.3$ at $Gr = 10^9$, $\tau = 500$: 1) $\lambda_{2,1} = 0.037$; 2) 0.0037.

Figure 9 shows the temperature profiles at $Gr = 10^8$ in the cross-section $Y = 0.3$. An increase in the heat conductivity coefficient of the wall material shows up as a temperature increase in the walls as well as in the region of the starting torch. Since the analyzed process is essentially nonstationary, it may be suggested that with increasing time the effect of increase in $\lambda_{2,1}$ will also affect the temperature increase in the gas cavity.

A decrease in the relative heat conductivity coefficient leads to an indefinitive change in the generalized heat transfer coefficient on the heat source surface (see Fig. 4). At $10^7 \le Gr < 7 \cdot 10^7$ $Nu_{avg}\big|_{\lambda_{2,1}=0.0037} > Nu_{avg}\big|_{\lambda_{2,1}=0.037}$ and $Gr \ge 7 \cdot 10^7$ $Nu_{avg}\big|_{\lambda_{2,1}=0.0037} < Nu_{avg}\big|_{\lambda_{2,1}=0.037}$ have been obtained. Such a change is due to the nonstationary interactions: the heat source intensity, on the one hand, and the heat removal through the enlosing solid walls, on the other.

In the range of $10^7 \le Gr < 7 \cdot 10^7$, an increase in λ_1 at $\tau = 600$ leads to an increase in the temperature gradient on the source surface, and, consequently, to a more intense outflow of the heat not only far into the cavity, but also into the enclosing walls. But already at $Gr \ge 7 \cdot 10^7$ the opposite is observed, which is due to the "polar" change in the influence of the convective heat transfer in the gas and the conductive heat transfer in the walls.

The profiles of the kinetic energy of turbulence and its dissipation rate in the cross-section $Y = 0.3$ with decreasing relative heat conductivity coefficient are given in Fig. 10. It should be noted that an increase in λ_1 leads to a shift of the local extremum of the K field and the E field to the right wall, which is analogous to the behavior of the starting torch.

Conclusions. We have solved numerically the problem of nonstationary turbulent natural convection in a closed square region with heat-conducting finite-thickness walls in the presence of a heat source with a constant temperature under the conditions of simultaneous radiative-convective heat exchange with the environment on one of the

outer boundaries. Distributions are obtained of the thermohydrodynamic parameters characterizing the features of the analyzed flow conditions and heat transfer $10^7 \le \mathrm{Gr} \le 10^9$, Pr = 0.7, and $\lambda_{2,1}$ = 0.037, 0.0037. We have performed a detailed analysis of the influence of the Grashof number, the nonstationarity factor, and the relative heat conductivity coefficient on both the local characteristics (streamlines, temperature field, field of the kinetic energy of turbulence, and its dissipation field) and the integral parameter (average Nusselt number on the heat source surface). It has been established that an increase in the Grashof number forms a more stable thermal torch inhibiting the advance of the lower-temperature front far into the cavity (Fig. 2). The nonstationarity factor tells on the redistribution of the analyzed local parameters (Fig. 5b). A decrease in the relative heat conductivity coefficient leads to a nonmonotonic change in the average Nusselt number on the heat source surface (Fig. 4).

It should be noted that simultaneous analysis of the streamlines and the temperature field makes it possible to estimate qualitatively the kinetic energy of turbulence and the rate of its dissipation.

This work was supported by the Russian Basic Research Foundation (grant No. 08-08-00402-a).

NOTATION

a, thermal diffusivity, m^2/sec; a_1, thermal diffusivity of the enclosing wall material, m^2/sec; a_t, turbulent thermal diffusivity, m^2/sec; $\mathrm{Bi}_1 = \alpha L/\lambda_1$, Biot number; $\mathrm{Bu} = \beta \Delta T$, Boussinesq number; E, dimensionless analog of the dissipation rate of the kinetic energy of turbulence; $\mathrm{Fo}_1 = a_1 t_0/L^2$, Fourier number of the material of the heat-conducting walls; $\mathrm{Gr} = \mathrm{Bu} g_y L^3/\nu^2$, Grashof number; $G_k = -\dfrac{1}{\mathrm{Re_t Pr_t}} \dfrac{\partial \Theta}{\partial Y}$, dimensionless term describing the generation of turbulent kinetic energy due to the buoyancy force; **g**, gravitational vector; g_y, component of the gravitational acceleration (g_x = 0), m/sec^2; h, distance from the nearest near-boundary unit to the wall, m; K, dimensionless analog of the kinetic energy of turbulence; k, kinetic energy of turbulence, m^2/sec^2; k_0, scale of the kinetic energy of turbulence, m^2/sec^2; L, gas cavity length, m; L_x, size of the solution region on the x axis, m; L_y, size of the solution region on the y axis, m; Nu_{avg}, average Nusselt number on the heat source surface; $P_k = \dfrac{1}{\mathrm{Re_t}} \left[2\left(\dfrac{\partial U}{\partial X}\right)^2 + 2\left(\dfrac{\partial V}{\partial Y}\right)^2 + \left(\dfrac{\partial U}{\partial X} + \dfrac{\partial V}{\partial X}\right)^2 \right]$, dimensionless term characterizing the generation of turbulence due to shear stresses; $\mathrm{Pr} = \nu/a$, Prandtl number; $\mathrm{Pr_t} = \nu_t/a_t$, turbulent Prandtl number; $\mathrm{Ra} = \mathrm{GrPr}$, Raleigh number; $\mathrm{Re} = E/(c_\mu K^2)$, turbulent Reynolds number; $\mathrm{Sk}_1 = \tilde{\varepsilon}\sigma L(\Delta T)^3/\lambda_1$, Stark number of the solid wall material; T, temperature, K; t, time, sec; t_0, time scale, sec; U, V, dimensionless velocities corresponding to velocities u, v; $V_0 = \sqrt{g_y \mathrm{Bu} L}$, velocity scale (velocity of natural convection); u, v, x, y, velocity components, respectively, m/sec; X, Y, dimensionless coordinates corresponding to coordinates x, y; x, y, Cartesian coordinates, m; α, heat exchange coefficient between the environment and the solution region under consideration, $W/(m^2 \cdot K)$; β, thermal volume expansion coefficient, K^{-1}; ε, dissipation rate of the kinetic energy of turbulence, m^2/sec^3; ε_0, scale of the dissipation rate of the kinetic energy of turbulence, m^2/sec^3; $\tilde{\varepsilon}$, reduced emissivity factor; Θ, dimensionless temperature; λ_i, heat conductivity coefficient of the ith subregion, $W/(m \cdot K)$; $\lambda_{2,1} = \lambda_2/\lambda_1$, relative heat conductivity coefficient; ν, kinematic molecular viscosity coefficient, m^2/sec; ν_t, kinematic molar (turbulent) viscosity coefficient, m^2/sec; ρ, gas density, kg/m^3; σ, Stefan–Boltzmann constant, $W/(m^2 \cdot K^4)$; τ, dimensionless time; Ψ, dimensionless analog of the stream function; ψ, stream function, m^2/sec; ψ_0, scale of the stream function, m^2/sec; Ω, dimensionless analog of the velocity vorticity vector; ω, velocity vorticity vector, $1/sec$; ω_0, scale of the velocity vorticity vector, $1/sec$. Subscripts: 0, initial instant of time; 1, solid material elements (Fig. 1); 2, gas cavity (Fig. 1); avg, average number; e, environment; h.s, heat source; t, turbulence parameter; i, j, material number; k, ordinal number of the coordinate system unit vector.

REFERENCES

1. Y. Jaluria, *Design and Optimization of Thermal Systems*, McGraw-Hill, New York (1998).
2. S. Sathe and B. Sammakia, A review of recent developments in some practical aspects of air-cooled electronic packages, *ASME J. Heat Transfer*, **120**, 830–839 (1998).
3. T. Icoz and Y. Jaluria, Design of cooling systems for electronic equipment using both experimental and numerical inputs, *ASME J. Elec. Packag.*, **126**, 465–471 (2005).
4. T. Icoz, N. Verma, and Y. Jaluria, Design of air and liquid cooling systems for electronic components using concurrent simulation and experiment, *ASME J. Elec. Packag.*, **128**, 466–478 (2006).
5. G. N. Dul'nev and N. N. Tarnovskii, *Thermal Regimes of Electronic Equipment* [in Russian], Énergiya, Leningrad (1971).
6. G. N. Dul'nev, *Heat and Mass Transfer in Radioelectronic Equipment* [in Russian], Vysshaya Shkola, Moscow (1984).
7. G. V. Biryulin, V. I. Egorov, Yu. Yu. Popov, and L. A. Savintseva, Thermal regime of microassemblies, in: *Scientific-Technical Bulletin of St. Petersburg State University and Heat and Mass Transfer Institute "Investigations and Developments in the Field of Physics and Instrument Making,"* Issue 31, 115–117 (2006).
8. L. G. Loitsyanskii, *Fluid Mechanics* [in Russian], Drofa, Moscow (2003).
9. Yu. A. Sokovishin and O. G. Martynenko, *Introduction to the Theory of Free-Convection Heat Transfer* [in Russian], Izd. LGU, Moscow (1982).
10. B. E. Launder and D. B. Spalding, The numerical computation of turbulent flows, *Comput. Meth. Appl. Mech. Eng.*, **3**, 269–289 (1974).
11. R. A. W. M. Henkes, Van Der Vlugt, and C. J. Hoogendoorn, Natural-convection flow in a square cavity calculated with low-Reynolds-number turbulence models, *Int. J. Heat Mass Transfer*, **34**, 377–388 (1991).
12. E. V. Bruyatskii, *Turbulent Stratified Jet Flows* [in Russian], Naukova Dumka, Kiev (1986).
13. A. L. Luikov, *Theory of Heat Conduction* [in Russian], Vysshaya Shkola, Moscow (1967).
14. N. Vardar, Numerical analysis of the transient turbulent flow in a fuel oil storage tank, *Int. J. Heat Mass Transfer*, **46**, 3429–3440 (2003).
15. H. Ozoe, A. Mouri, M. Ohmuro, S. W. Churchill, and N. Lior, Numerical calculations of laminar and turbulent natural convection in water in rectangular channels heated and cooled isothermally on the opposing vertical walls, *Int. J. Heat Mass Transfer*, **28**, 125–138 (1985).
16. K. J. Hsieh and F. S. Lien, Numerical modeling of buoyancy-driven turbulent flows in enclosures, *Int. J. Heat Fluid Flow*, **25**, 659–670 (2004).
17. V. M. Paskonov, V. I. Polezhaev, and L. A. Chudov, *Numerical Simulation of Heat and Mass Transfer Processes* [in Russian], Nauka, Moscow (1984).
18. A. A. Samarskii, *Theory of Difference Schemes* [in Russian], Nauka, Moscow (1977).
19. H. N. Dixit and V. Babu, Simulation of high Rayleigh number natural convection in a square cavity using the lattice Boltzmann method, *Int. J. Heat Mass Transfer*, **49**, 727–739 (2006).
20. P. Le Quere, Accurate solutions to the square thermally driven cavity at high Rayleigh number, *Comput. Fluids*, **20**, 29–41 (1991).
21. S. M. Elsherbiny, G. D. Raithby, and K. G. T. Hollands, Heat transfer by natural convection across vertical and inclined layers, *ASME J. Heat Transfer*, **104**, 96–102 (1982).
22. Y. Jaluria, *Natural Convection: Heat and Mass Transfer* [Russian translation], Mir, Moscow (1983).